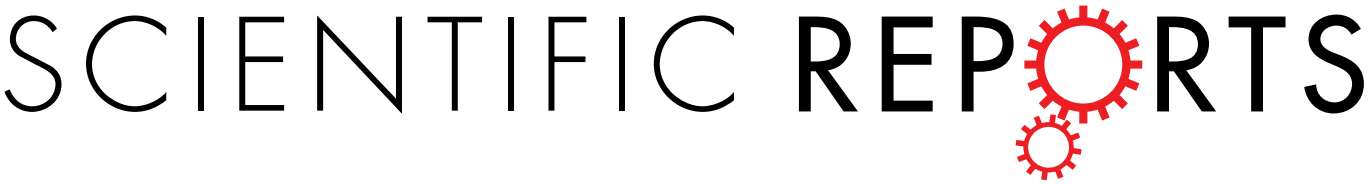

OPEN

Received: 20 September 2016
Accepted: 07 November 2016
Published: 05 December 2016

Apparent Negative Reflection with the Gradient Acoustic Metasurface by Integrating Supercell Periodicity into the Generalized Law of Reflection

Bingyi Liu[1], Wenyu Zhao[1] & Yongyuan Jiang[1,2]

As the two dimensional version of the functional wavefront manipulation metamaterial, metasurface has become a research hot spot for engineering the wavefront at will with a subwavelength thickness. The wave scattered by the gradient metasurface, which is composed by the periodic supercells, is governed by the generalized Snell's law. However, the critical angle that derived from the generalized Snell's law circles the domain of the incident angles that allow the occurrence of the anomalous reflection and refraction, and no free space scattering waves could exist when the incident angle is beyond the critical angle. Here we theoretically demonstrate that apparent negative reflection can be realized by a gradient acoustic metasurface when the incident angle is beyond the critical angle. The underlying mechanism of the apparent negative reflection is understood as the higher order diffraction arising from the interaction between the local phase modulation and the non-local effects introduced by the supercell periodicity. The apparent negative reflection phenomena has been perfectly verified by the calculated scattered acoustic waves of the reflected gradient acoustic metasurface. This work may provide new freedom in designing functional acoustic signal modulation devices, such as acoustic isolator and acoustic illusion device.

Tailoring the wavefront into arbitrary desired shape with a metasurface, the two dimensional metamaterial with subwavelength inclusions, has attracted tremendous attention in recent years. Since metasurface itself can be regarded as the application of the Huygens' principle, arbitrary wavefront manipulation can be realized by designing these artificial secondary sources according to the detailed information of the desired wavefront. The milestone work done by *Yu, N et al.*[1] stimulates the intensive investigation about the electromagnetic metasurfaces and reveals the huge potentials underneath the metasurface of realizing highly integrated functional electromagnetic devices, such as the planar lens[2,3], optical vortex generator[4,5], holograms[6,7] and ultrathin cloaking[8,9]. Some non-trivial physical phenomenon, such as the photonic spin Hall effect[10,11] and the generalized laws of reflection and refraction[1,12,13] to name a few, can be amply studied with the help of the gradient metasurfaces. Similar to their electromagnetic counterparts, acoustic metasurfaces have become attractive for they are able to engineer the phase profiles of the impinging waves by the artificial designed structures with subwavelength thickness instead of the space consuming solutions offered by the traditional diffractive acoustic devices. Numerous types of acoustic meta-atoms have been proposed to construct the functional acoustic metasurfaces, such as tapered labyrinthine structure[14], coiling-up slit structure[15,16], zigzag channel[17], Helmholtz resonator array[18], split sphere[19] and membrane based structure[20]. Based on these acoustic meta-atoms, a great number of acoustic wavefront manipulation devices have been constructed and operated successfully, for example, the acoustic focusing lens[21,22], acoustic vortex beam generator[23], acoustic Airy beam generator[24,25], acoustic carpet cloaking[26,27] and so on.

Gradient metasurface is a periodic array of the supercell with a linearly varying phase modulation ranging from 0 to 2π, and the wave scattered by the gradient metasurface is governed by the generalized laws of reflection

[1]Department of Physics, Harbin Institute of Technology, Harbin 150001, China. [2]Key Lab of Micro-Optics and Photonic Technology of Heilongjiang Province, Harbin 150001, China. Correspondence and requests for materials should be addressed to Y.J. (email: jiangyy@hit.edu.cn)

and refraction. According to the generalized laws of reflection and refraction, there exists a critical angle which defines the domain that the anomalous reflection or refraction can occur, and beyond the region defined by the critical angle the incident beam would be transformed into the surface bounded wave, and thus the metasurface works as the anti-scattering coating[28,29]. However, a recent study about the transmissive acoustic metasurface reports the observation of the apparent negative refraction when the incident angle is beyond the critical angle[30] and a review paper also covers some detailed discussion about this interesting phenomena[31]. The apparent negative refraction investigated by *Xie Y. et al.* can be understood by revisiting the influence of the supercell periodicity as well as the local phase modulation on the acoustic gradient metasurface. Thereafter, a more comprehensive discussion about the negative refraction that occurs in optical region when the incident angle is beyond the critical angle has been demonstrated[32]. However, *Xie Y. et al.*[30] only study the apparent negative refraction corresponding to a specific high diffraction order and no more discussion about the reflection behaviors of such gradient acoustic metasurface. Therefore, the reflection behaviors of a reflected gradient acoustic metasurface beyond the critical angle is of great interest to be studied.

In this paper, we theoretically study the influences of the supercell periodicity on the reflection behaviors of the gradient acoustic metasurface. The apparent negative reflection occurs when the incident angle is beyond the critical angle, which has been perfectly verified by the calculated reflected acoustic field of the reflected gradient acoustic metasurface. The theoretical study shows that the generalized law of reflection still works within the region defined by the critical angle, however, when the incident angle is beyond the critical angle, the generalized law of reflection would be modified with the reciprocal lattice vector corresponding to the higher order diffraction. As for the possible higher order diffraction, it depends on the amplitude of the metasurface's surface phase gradient and the incident angle, which can be regarded as a more general case discussed in ref. 30.

Results

The generalized law of reflection for full-angle incidence and arbitrary gradient metasurface.

Since the gradient metasurface introduces the phase discontinuity across the scattered interface, the local graded phase modulation of the periodic supercell resets the classical Snell's law by adding a surface phase gradient term which now is known as the generalized law of reflection and refraction. For a reflected gradient metasurface with a surface phase gradient $\xi = \nabla\varphi_s$, where φ_s is the position dependent reflected phase modulation along the gradient metasurface, the generalized law of reflection provides a complete description about the reflection behaviors of the metasurface under the plane wave illumination:

$$(\sin\theta_{re} - \sin\theta_i)k_0 = \xi \tag{1}$$

where θ_i is the incident angle, θ_{re} is the anomalous reflected angle and k_0 is the amplitude of the free space wave vector. Since the gradient metasurface offers a linear phase modulation from 0 to 2π over a supercell period, the surface phase gradient term can be further written as $\xi = \sigma\frac{2\pi}{p_s}$, where p_s is the supercell period length and $\sigma = 1$ or -1, which indicates the direction of the surface phase gradient. According to formula (1), the critical angle $\theta_c = \mathrm{sgn}(\xi)\arcsin\left(1 - \left|\frac{\xi}{k_0}\right|\right)$ can be solved mathematically and it defines the domain of the incident angles that satisfy the momentum matching condition along the metasurface. The gradient metasurface has a saw tooth phase modulation profile, which is exactly coincident with that of a blazed diffraction grating, and thus the anomalous reflected beam can be regarded as the $+1$ order diffraction as well[33]. However, the gradient metasurface is a periodic array of the inhomogeneous supercells, the non-local effect that originates from the supercell periodicity should be considered as an indispensable factor when we want to have a comprehensive understanding of the wavefront manipulation behaviors of a gradient metasurface. In this case, the generalized law of reflection can be rewritten as (exactly the same form of the formula between the incident angle and refracted angle for a transmissive gradient metasurface placed in homogeneous background medium[30])

$$(\sin\theta_{re} - \sin\theta_i)k_0 = \xi + n_G G \tag{2}$$

where $G = \frac{2\pi}{p_s}$ is the amplitude of the reciprocal lattice vector, and n_G indicates the corresponding diffraction order. According to the classical diffraction theory, n_G is equal to 0 as long as the incident angle is inside the region defined by the formula (1). When the incident angle is beyond the critical angle, n_G would take some other values to maintain the validity of formula (2) (for example, $n_G = -3$ in ref. 30), that means the anomalous reflection or the apparent negative reflection occurs.

For an electromagnetic metasurface composed by the gradient metallic subunits, the surface bounded wave, which is stimulated by the beam of the incident angle that is beyond the critical angle, would be wore down and transformed into the joule heat because of the intrinsic loss of the metasurface[28,29]. However, the acoustic energy loss along with the interaction between the incident acoustic waves and metasurface structure is determined by the background medium loss caused by medium viscosity and thermal acoustic effects. In this paper, we focus on the reflected acoustic gradient metasurface made of hard material under audible airborne (2.5 kHz) acoustic wave illumination. The significance of the influences of the viscosity and thermal acoustic effects are determined by whether the minimal geometrical parameter (for example, the width of the channel) is comparable to the acoustic boundary layer thickness or not[34]: the viscous boundary $d_v = \sqrt{\frac{2\mu}{\omega\rho}}$ and thermal boundary $d_{th} = \sqrt{\frac{2\kappa}{\omega\rho C_p}}$, where μ is the dynamic viscosity of air, κ is the thermal conduction coefficient of air, ρ is the density of air, C_p is the specific heat at constant pressure, and ω is the angular frequency. In this paper (2.5 kHz, 20 °C, 1 atm.), $d_v = 0.044$ mm, $d_{th} = 0.05$ mm and the minimal geometrical size is 1 mm (the thickness of the neck slit, detailed information about the meta-atoms we utilize for the full-wave simulation is presented in the following content, see Fig. 1(a)).

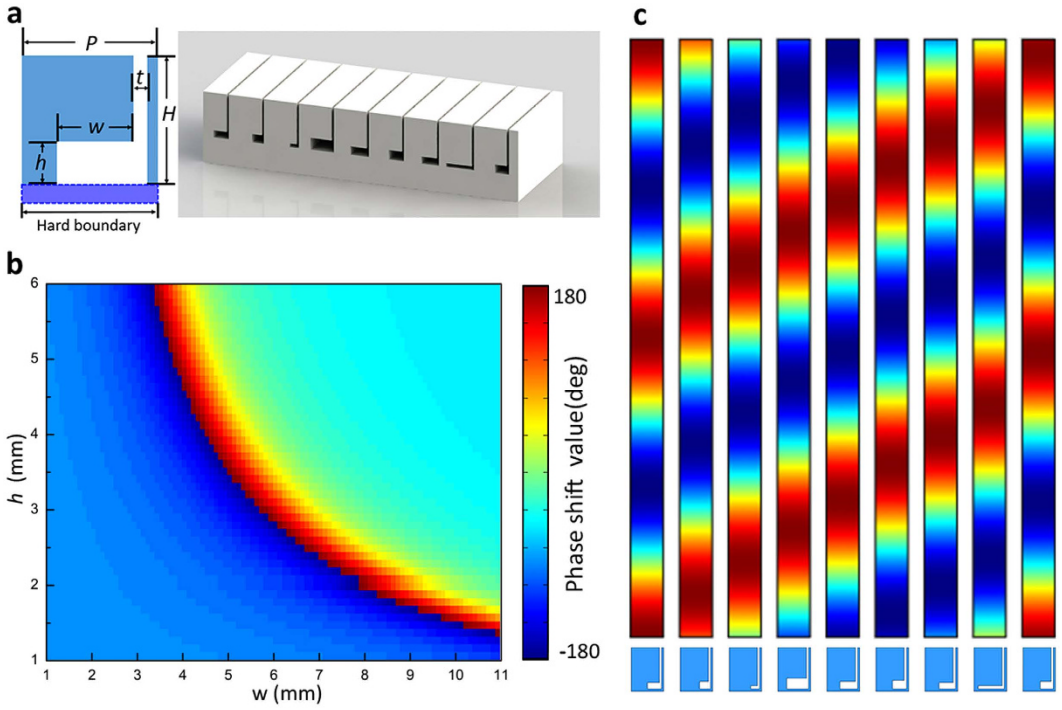

Figure 1. Design of the functional acoustic meta-atoms. (**a**) Schematic demonstration of the designed subunit sample and a typical supercell consists of 9 subunits. (**b**) Phase shift values map of the subunits of varying cavity width w and height h. Here, the subunit width $P = 15$ mm, neck thickness $t = 1$ mm and neck height $H = 19$ mm. (**c**) Scattered acoustic field of a typical set of subunits with a linearly varying phase modulation ranging from 0 to 2π.

Therefore, the intrinsic loss of the gradient acoustic metasurface can be regarded as a negligible factor when dealing with the interaction between the impinging waves and metasurface structures. Because of the low energy loss, the acoustic surface bounded waves would efficiently interact with the intrinsic Floquet-Bloch modes offered by the gradient metasurface's periodic supercell array, and reradiate into the free space which finally leads to the apparent negative reflection governed by formula (2).

Design of the reflected gradient metasurface for airborne sound. Following the strategy of engineering the impedance profile of the acoustic metasurface, we utilize the Helmholtz resonator with a L shape cavity as the building block to construct the desired reflected acoustic gradient metasurface. Figure 1(a) demonstrates one meta-atom sample and a typical gradient supercell composed by nine subunits which corresponds to a linear phase shift covering the full 2π range. The L shape Helmholtz resonator can be regarded as a combination of the following two parts: a vertical thin neck channel of thickness t and height H, a resonant cavity of height h and width w. In this paper, the metasurface is designed to operate under 2.5 kHz airborne acoustic wave illumination and the subunit is made of nylon which is stiff enough to treat the interaction boundary as the hard boundary. Then we calculate the scattered acoustic field of the periodic array of a single subunit, which is excited by a normally incident plane acoustic wave, and vary the height as well as the width of the bottom cavity to obtain a complete phase modulation map of the L shape Helmholtz resonator (see Fig. 1(b)). Figure 1(c) illustrates the scattered pressure field of nine subunits with the linearly varying phase modulation ranging from 0 to 2π, and the scattered field is normalized by the amplitude of the background field.

Simulation verification of the apparent negative reflection. To verify the validity of our theoretical prediction about the apparent negative reflection, the high order diffraction that occurs when the incident angle is beyond the critical angle, we investigate the reflection behaviors of four reflected acoustic gradient metasurfaces with different supercell periods. In this work, we assume that the reciprocal lattice vector G heads to the same direction with the surface phase gradient ξ and n_G is a nonpositive integer. Therefore, $\xi = G = \sigma\frac{2\pi}{p_s}$, formula (2) can be rewritten as

$$\sin\theta_{re} - \sin\theta_i = (1 + n_G)k_s \tag{3}$$

where $k_s = \frac{\xi}{k_0}$ denotes the reduced surface gradient. Based on formula (3), the wave reflection behaviors of the gradient metasurface can be straightforward demonstrated by depicting the relation between $\sin\theta_i$ and $\sin\theta_{re}$. Figure 2(a) illustrates a general case of the apparent negative reflection of the reflected gradient acoustic metasurface. The orange dash line circles the domain of all possible ($\sin\theta_i$, $\sin\theta_{re}$) solutions of the allowed k_s, and the generalized law of reflection that is amended by the reciprocal lattice vector of the supercell period can be visually

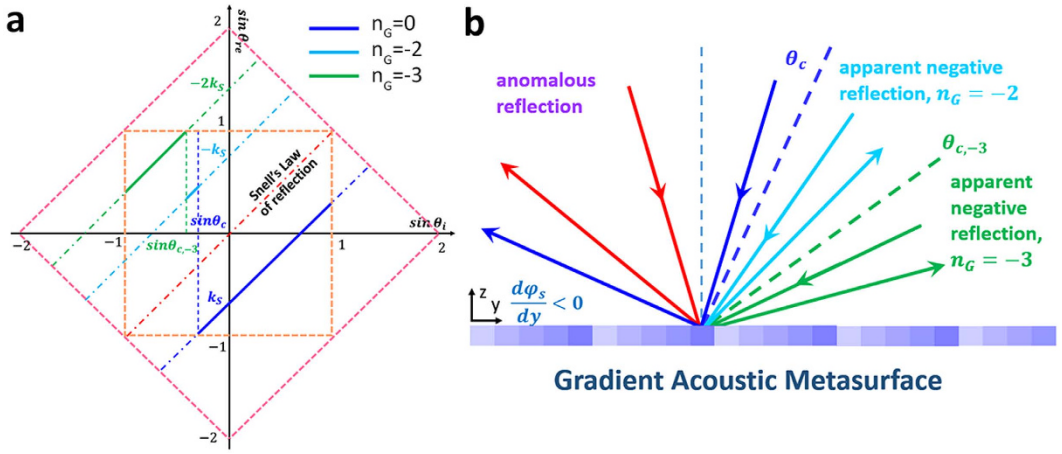

Figure 2. Schematic demonstration of the general case of the apparent negative reflection with the gradient acoustic metasurface. (**a**) Relation between $\sin\theta_i$ and $\sin\theta_{re}$. The blue, cyan and green solid line correspond to n_G takes the value of 0, −2 and −3 respectively, which represent the intrinsic anomalous reflection state $|0\rangle$ and the another two allowed apparent negative reflection states $|-2\rangle$ and $|-3\rangle$ correspondingly. The red dotted line represents the specular reflection state $|-1\rangle$, which is forbidden here. The orange dotted square circles the domain of all possible reflection states and the pink dotted square defines the all allowed phase gradient shift that maintains the anomalous wavefront manipulation characteristic of the gradient metasurface, when the amplitude of the surface phase gradient is greater than $2k_0$, the structured gradient metasurface works as a uniform flat impedance ground. (**b**) Schematic illustration of the anomalous reflection (red and blue solid beam), the apparent negative reflection taking place beyond the critical angle θ_c when $n_G = -2$(cyan solid beam) and $n_G = -3$(green solid beam).

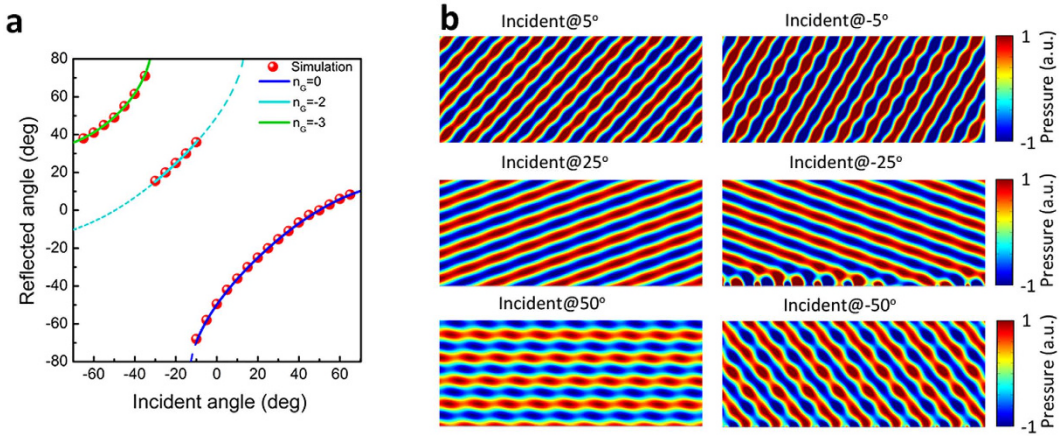

Figure 3. The apparent negative reflection behavior of the gradient acoustic metasurface when $\xi = -0.762\,k_0$. (**a**) The relation between the incident angle and reflected angle when $k_s = -0.762$. The red dots are data obtained from the full-wave simulation. The blue solid line indicates the anomalous reflection state $|0\rangle$, the cyan and green solid lines represent the allowed apparent negative reflection states $|-2\rangle$ and $|-3\rangle$ respectively. (**b**) Calculated scattered acoustic field under the plane acoustic wave illumination of different incident angles.

demonstrated as shifting the Snell's law of reflection within the region encompassed by the pink dashed square as well. The blue solid line shown in Fig. 2(a) indicates the anomalous reflection governed by the generalized law of reflection when the incident angle is within the critical angle. Things turn out to be interesting when the incident angle is beyond the critical angle θ_c, the surface bounded waves supported by the linear local phase modulation of the subunits would interact with the Floquet-Bloch modes offered by the supercell lattices and reradiate into the free space as the high order diffractions. Under this case, the relation between the incident angle and reflected angle can be described by formula (3), and there could be several possible n_G values as long as the momentum matching condition over the metasurface is satisfied. It is apparent that the reduced surface phase gradient k_s of smaller absolute value will have more possible n_G values, and thus, to simplify our discussion, we firstly study the case that $0.5 < |k_s| < 1$. In this situation, all possible n_G values can be solved by maintaining the validity of

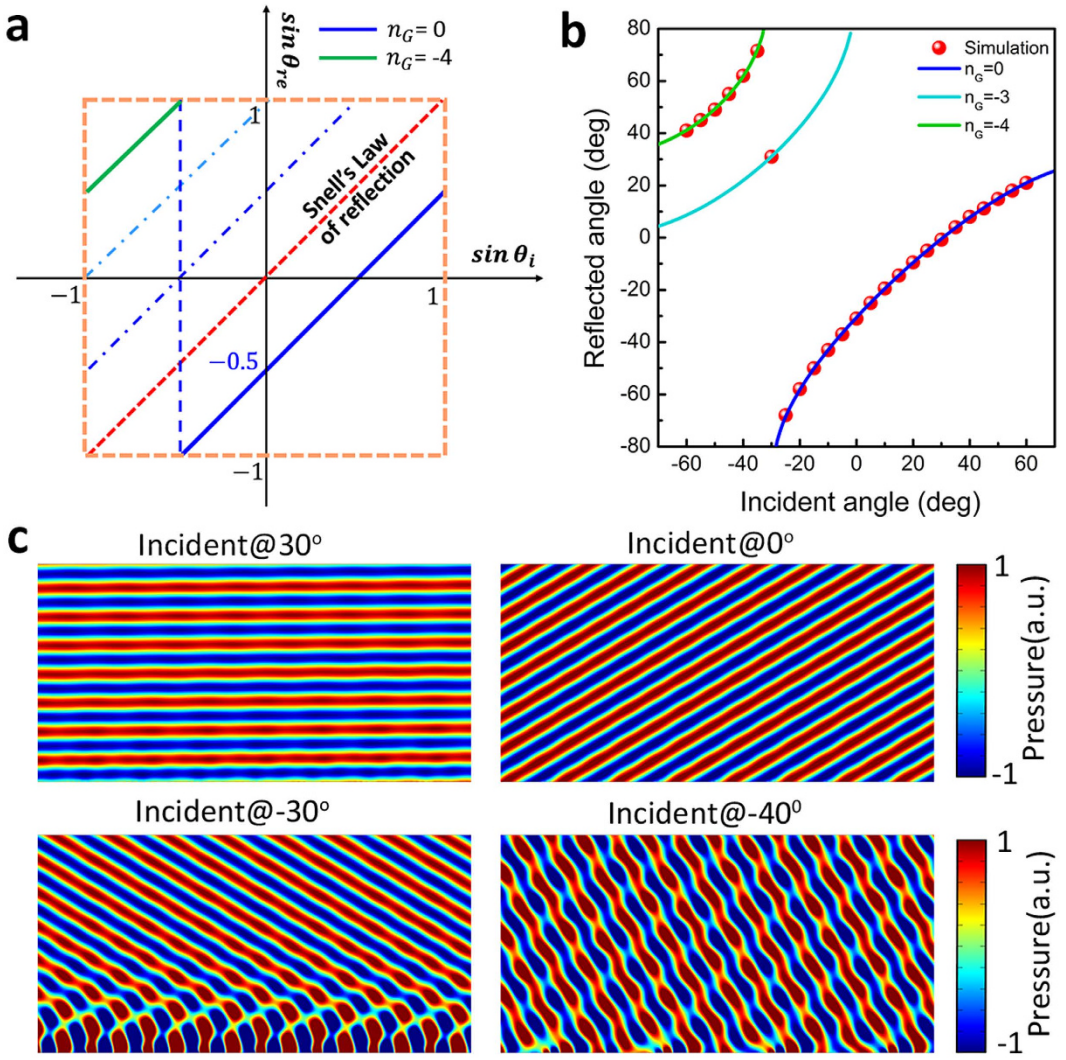

Figure 4. The apparent negative reflection behavior of the gradient acoustic metasurface when $\xi = -0.508\,k_0$. (**a**) Relation between $\sin\theta_i$ and $\sin\theta_{re}$ when $k_s = -0.508$. The blue solid line indicates the anomalous reflection state $|0\rangle$, the green solid line represents the allowed apparent negative reflection $|-4\rangle$. The red dotted line represents the specular reflection $|-1\rangle$, the blue and cyan dash-dot line correspond to the forbidden apparent reflection state $|-2\rangle$ and $|-3\rangle$. (**b**) The relation between the incident angle and reflected angle when $k_s = -0.508$. (**c**) Calculated reflected acoustic field of the gradient acoustic metasurface when $k_s = -0.508$. When the acoustic plane wave is incident at 30°, 0°, −30° and −40°, the beam would reflect at −0.8°, −31°, 31° and 62° correspondingly.

formula(3) and consequently n_G could take the value of 0, −1, −2 and −3. Since the lateral wave vector component of the impinging wave $k_{\parallel} = k_0 \sin\theta_i$ is incident angle dependent, the choice of n_G value would be incident angle dependent as well. When the incident angle gradually varies from 90° to −90°, the value of n_G can be determined by the 'jump-up' rule in our paper. Here we firstly treat the reflection behaviors of the gradient acoustic metasurface as several reflection states $|n_G\rangle$, i.e., state $|0\rangle$ corresponds to the anomalous reflection governed by the generalized law of reflection, state $|-1\rangle$ corresponds to the specular reflection which indicates that the gradient metasurface has no anomalous manipulation effects on the impinging waves, state $|-2\rangle$ and $|-3\rangle$ correspond to the allowed apparent negative reflections involving the higher order diffractions. When the incident angle θ_i varies beyond the critical angle θ_c, reflection state $|0\rangle$ would be switched into reflection state $|-1\rangle$, $|-2\rangle$ and $|-3\rangle$. This switching procedure can be qualitative understood as the energy of the acoustic surface bounded wave redistributes into higher order diffractions via the scattering effects introduced by the supercell lattices, and within a narrow region around the critical angle, several reflection states could coexist but differ in intensity (detailed discussion is presented in Discussion part). However, the transition between different reflection states when the incident angle varies monotonously around the critical angle is relative drastic, and that is why we describe the switch between the reflection states as 'jump-up'. It should be noted that when the incident angle domain of two allowed reflection states overlap (exclude the reflection state $|0\rangle$), the allowed reflection state of larger absolute n_G

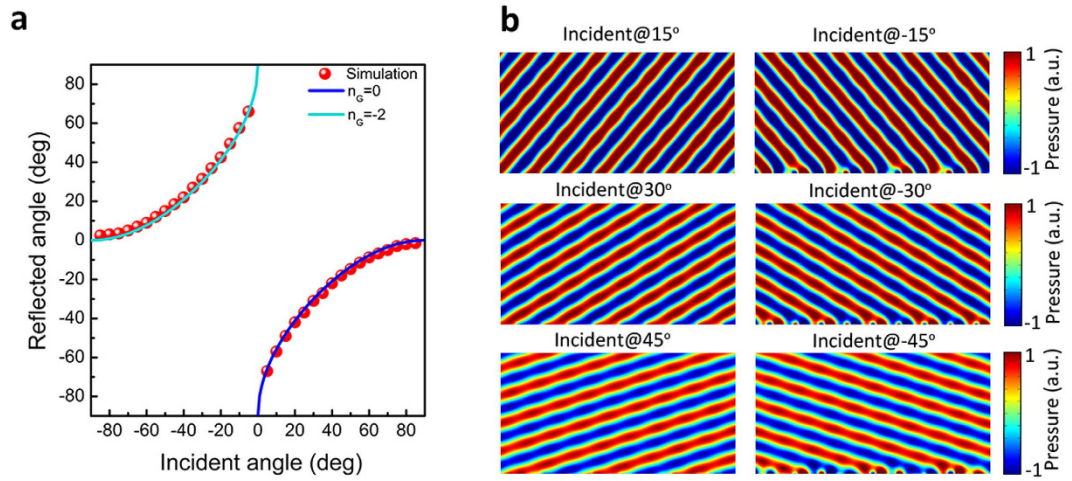

Figure 5. The apparent negative reflection behavior of the gradient acoustic metasurface when $\xi = -1.016k_0$. (**a**) The relation between the incident angle and reflected angle when $k_s = -1.016$. (**b**) Calculated scattered acoustic field under the plane acoustic wave illumination of different incident angle values when $k_s = -1.016$. The acoustic plane wave is incident at 15°, −15°, 30°, −30°, 45° and −45°, the beam would reflect at −49°, 49°, −31°, 31°, −18° and 18° correspondingly.

value would be superior to that of a smaller one. For example, Fig. 2(a) illustrates the situation that when the incident angle varies beyond the critical angle, the anomalous reflection state $|0\rangle$ jumps to the apparent negative reflection state $|-2\rangle$ but not the mirror reflection state $|-1\rangle$, because the incident angle domain of mirror reflection state $|-1\rangle$ overlaps with the state $|-2\rangle$. Similarly, when the incident angle is beyond the shift critical angle $\theta_{c,-3}$ (the mathematically allowed critical angle for the corresponding high order diffraction), the apparent negative reflection state $|-2\rangle$ would jump to the apparent negative reflection state $|-3\rangle$ for the same reason. Figure 2(b) schematically depicts the anomalous reflection behaviors of the gradient acoustic metasurface that supports $|0\rangle$, $|-2\rangle$ and $|-3\rangle$ reflection state simultaneously.

Figure 3 demonstrates the apparent negative reflection behaviors of the gradient acoustic metasurface with the reduced surface phase gradient $k_s = -0.762$. The critical angle θ_c is solved to be −13.8° and the shift critical angle $\theta_{c,-3}$ can be calculated by $\theta_{c,-3} = arcsin(1 + 2k_s) = -31.6^\circ$. When $-13.8° < \theta_i < 90°$, the reflected angle can be predicted by $\theta_{re} = arcsin(k_s + \sin\theta_i)$, just as the blue solid line presented in Fig. 3(a). When $-31.6° < \theta_i < -13.8°$, the Floquet-Bloch mode with 2G propagation constant amplitude would strongly scatter the surface bounded waves and forms the free space propagating waves, the reflected angle can be solved by $\theta_{re} = arcsin(-k_s + \sin\theta_i)$. Similarly, when $-90° < \theta_i < -31.6°$, the Floquet-Bloch mode with 3G propagation constant amplitude scatters the surface bounded waves intensively and the reflected angle $\theta_{re} = arcsin(-2k_s + \sin\theta_i)$. Obviously, the reflected angles that obtained from the calculated far field distribution agree well with the values calculated by formula (3). Figure 3(a) shows the apparent negative reflections corresponding to $n_G = -2$ and $n_G = -3$, Fig. 3(b) shows the calculated reflected acoustic field corresponding to different incident angles, when the plane acoustic wave is incident at 5°, −5°, 25°, −25°, 50° and −50° respectively, the beam would reflect at −42°, −58°, −20°, 20°, 0°, and 49° correspondingly.

Considering the situation that $|k_s| \leq 0.5$, even larger absolute value of n_G is allowed. For example, when $k_s = -0.5$, there are five possible reflection states: $|0\rangle$, $|-1\rangle$, $|-2\rangle$, $|-3\rangle$, $|-4\rangle$. Based on the 'jump-up' rule, the anomalous reflection state would jump to the apparent negative reflection state $|-4\rangle$ when the incident angle is beyond the critical angle (see Fig. 4(a)), because the shift critical angle $\theta_{c,-4} = arcsin(1 + 3k_s)$ is equal to the critical angle θ_c. Figure 4(b) shows the well agreement between the simulation results and theoretical calculated values. And it can be seen from the picture that the apparent negative reflection state $|-3\rangle$ still exists, the possible reason is that the normalized surface phase gradient value of the gradient acoustic metasurface is chosen as $k_s = -0.508$, which slightly diverts from −0.5, for the full-wave simulation. However, such minor difference would shift $\theta_{c,-4}$ form −30° to −31.6° and θ_c from −30° to −29.5°, and thus the apparent negative reflection state $|-3\rangle$ could survive in a narrow domain. Figure 4(c) shows the calculated acoustic field when the plane acoustic waves illuminate from different directions.

When $|k_s| = 1$, only three possible reflection states are allowed: $|0\rangle$, $|-1\rangle$ and $|-2\rangle$. Since the shift critical angle is $\theta_{c,-2} = \theta_c = 0^\circ$, thus the anomalous reflection state $|0\rangle$ would directly jump to the apparent negative reflection state $|-2\rangle$ when the incident angle is beyond the critical angle, or equally saying that the surface bounded waves would strongly interact with the Floquet-Bloch mode of 2 G propagation constant amplitude, and form the apparent negative reflection beam. The center symmetrical reflected angle distribution shown in Fig. 5(a) suggests that the full-angle negative reflection can be realized by such gradient acoustic metasurface, of which the amplitude of the surface phase gradient is equal to the free space wave vector k_0. When $\theta_i \geq 0$, the reflected angle can be solved by $\theta_{re} = sgn(k_s)arcsin(1 - |k_s|)$ and when $\theta_i < 0$, the reflected angle is $\theta_{re} = -sgn(k_s)arcsin(1 - |k_s|)$.

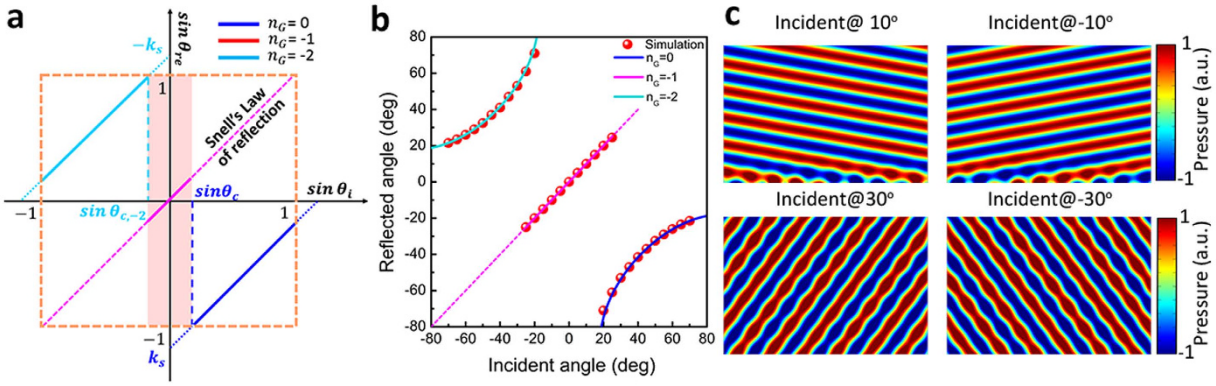

Figure 6. The apparent negative reflection behavior of the gradient acoustic metasurface when $\xi = -1.307\,k_0$. (**a**) The relation between $\sin\theta_i$ and $\sin\theta_{re}$ when $k_s = -1.307$. The blue solid line represents the anomalous reflection $|0\rangle$, the pink solid line represents specular reflection $|-1\rangle$ and the cyan solid line represents the apparent negative reflection $|-2\rangle$. (**b**) The relation between the incident angle and reflected angle when $k_s = -1.307$. (**c**) Calculated scattered acoustic field under the plane acoustic wave illumination of different incident angle values when $k_s = -1.307$. The acoustic plane wave is incident at 10°, −10°, 30° and −30°, and the beam reflects at 10°, −10°, −53° and 53° correspondingly.

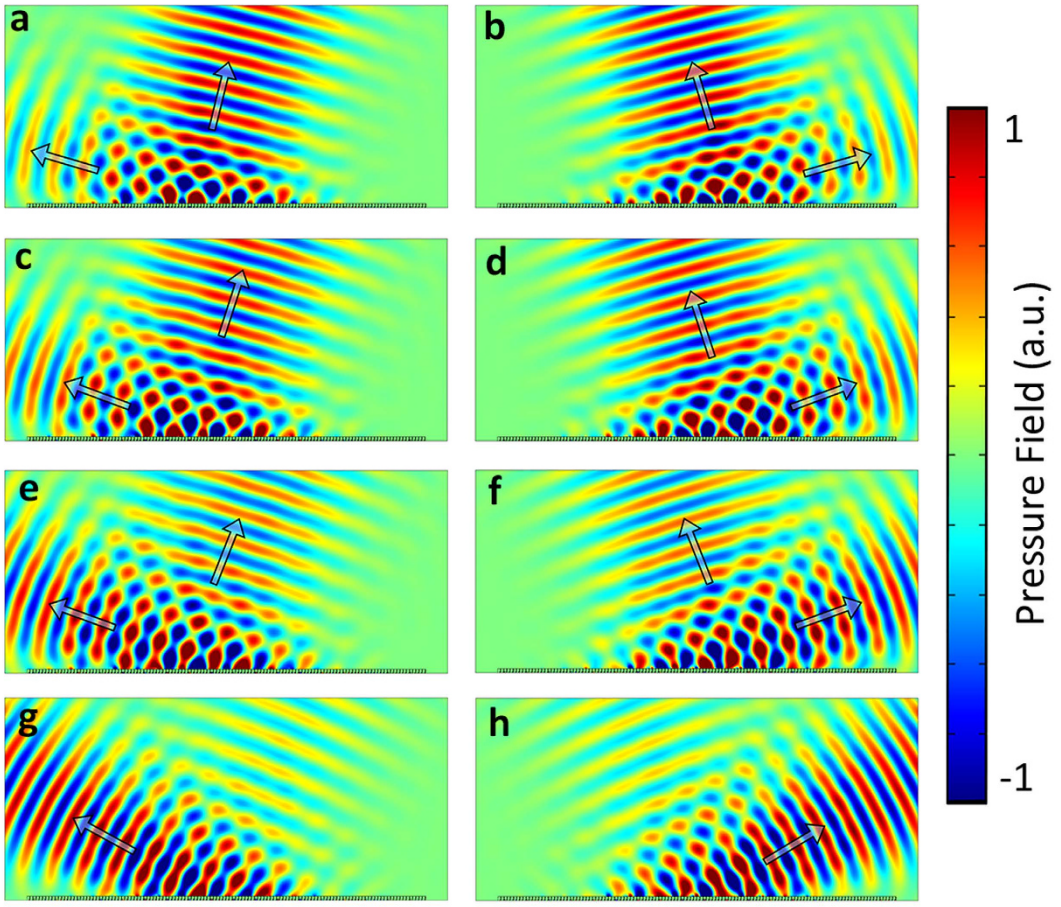

Figure 7. The calculated scattered acoustic field when the acoustic Gaussian beam impinges onto a finite gradient metasurface composed by 18 supercells, each supercell consists of 7 subunits which corresponds to a $-1.307\,k_0$ surface phase gradient. (**a**)~(**h**) are the scattered field when the incident angle is 15°, −15°, 17°, −17°, 20°, −20°, 25° and −25° respectively.

Figure 5(b) is the calculated reflected acoustic field under the illumination of the acoustic plane waves with different incident angles.

When $1 < |k_s| < 2$, there are three possible reflection states: $|0\rangle, |-1\rangle$ and $|-2\rangle$. Figure 6 illustrates the reflection behaviors of the gradient acoustic metasurface with $k_s = -1.307$. The shift critical angle is $\theta_{c,-2} = -17.9°$ while the critical angle is $\theta_c = 17.9°$. And the anomalous reflection state $|0\rangle$ will firstly jump to the mirror reflection state $|-1\rangle$, and then from state $|-1\rangle$ jumps to the apparent negative reflection state $|-2\rangle$ (see Fig. 6(a)). Such reflection manipulation behavior is the typical wide-angle negative reflection phenomena[35]. Figure 6(b) is the reflected angle distribution when incident angle varies from 80° to −80°. Figure 6(c) is the calculated reflected acoustic field distribution when the plane acoustic waves are incident at different angles. When $|k_s| \geq 2$, the metasurface has no manipulation effect on the incident beam and only mirror reflection occurs.

Discussion

The 'jump' between the different reflection states is the redistribution of the reflected acoustic energy of different diffraction orders, which originates from the interaction between the surface bounded waves and the effect of the non-local supercell period. It can be seen from the calculated reflected acoustic field corresponding to the apparent negative reflection, the total scattered field is the superposition of a surface bounded waves and the free space propagation wave (see Fig. 5(b)). When we vary the incident angles around the critical angle or the shift critical angle, we can observe a gradual evolution of the redistributed acoustic energy between different reflection states. For example, Fig. 6(b) indicates that when the incident angle locates around the critical angle θ_c or the shift critical angle $\theta_{c,-2}$, one incident angle could correspond to two reflected angles simultaneously, because the two reflection states have the comparable field intensity on this occasion. Figure 7 shows a more straightforward illustration of the energy redistribution between different reflection states when an acoustic Gaussian beam of gradually varying incident angles impinges upon the gradient metasurface of the finite length (the energy redistribution between the anomalous reflection state $|0\rangle$ and the specular reflection state $|-1\rangle$ around the critical angle θ_c, see Fig. 7(a),(c),(e) and (g); the energy redistribution between the specular reflection state $|-1\rangle$ and apparent negative reflection $|-2\rangle$ around the shift critical angle $\theta_{c,-2}$, see Fig. 7(b),(d),(f) and (h)).

It should be noted that such apparent negative reflection and the anomalous reflection phenomenon of the gradient acoustic metasurface could distort the scattered field of the object encompassed by it and thus the gradient acoustic metasurface has the potential to be applied as the illusion devices. Furthermore, the full-angle negative reflection phenomena illustrated in Fig. 5 indicates the unique trait of an acoustic insulator: when two acoustic beams are incident from opposite direction, the reflected beams locate at the same quadrant with the incident beam, therefore, two reflected beams would not encounter.

Conclusion

In summary, we demonstrate the apparent negative reflection phenomenon that takes place when the incident angle is beyond the critical angle, which should be forbidden according to the generalized law of reflection, can be realized with the reflected gradient acoustic metasurface. The underlying mechanism of such anomalous phenomenon can be understood by treating the apparent negative reflection as the high order diffraction which is produced via the interaction between the surface bounded waves and the supercell periodicity. Integrating the reciprocal lattice vector term, which represents the influences of the supercell periodicity, to the generalized law of reflection offers perfect prediction about the reflected angle values of the apparent negative reflection. Full-wave simulation of the scattered acoustic fields of the gradient acoustic metasurface illustrates versatile apparent negative reflection phenomenon perfectly, and the nontrivial full-angle negative reflection, which combines the anomalous reflection and the apparent negative reflection behaviors of the gradient acoustic metasurface, offers a simple way for isolating the acoustic waves incident from opposite directions. This study may provide more freedom for designing the acoustic signal modulation devices and the potential applications in acoustic beam steering.

Methods

In this paper, we take advantage of the Finite Element Method (FEM) based on the commercial software COMSOL Multiphysics to conduct the full-wave simulations. The acoustic pressure model is used, the background medium is set to be air and the corresponding acoustic speed is chosen as 343 m/s. The gradient metasurface is studied as the infinite period by applying the periodic boundary condition on the right and left sides of the simulation region. The reflected angle is obtained according to the far-field acoustic pressure distribution. As for the influences of the viscosity and thermal acoustic effects on the reflection behaviors of the metasurface, we utilize two different methods to testify the robustness of the apparent negative reflection by introduce an imaginary part to the acoustic refractive index of the air ($n = 1 - 0.1i$) or directly apply the thermal acoustic model within the metasurface structures to conduct the full-wave simulation. The calculated reflected acoustic fields obtained by the above methods are almost same with the results that calculated without considering the dissipative loss.

References

1. Yu, N. *et al.* Light propagation with phase discontinuities: generalized laws of reflection and refraction. *Science* **334,** 6054 (2011).
2. Aieta, F. *et al.* Aberration-free ultrathin flat lenses and axicons at telecom wavelengths based on plasmonic metasurfaces. *Nano Lett.* **12,** 4932–4936 (2012).
3. Lin, M., Fan, P., Hasman, E. & Brongersma, M. L. Dielectric gradient metasurface optical elements. *Science* **345,** 6194 (2014).
4. Genevet, P. *et al.* Ultra-thin plasmonic optical vortex plate based on phase discontinuities. *Appl. Phys. Lett.* **100,** 013101 (2012).
5. Mehmood, M. Q. *et al.* Visible-frequency metasurface for structuring and spatially multiplexing optical vortices. *Adv. Mater.* **28,** 2533–2539 (2016).
6. Huang, L. *et al.* Three-dimensional optical holography using a plasmonic metasurface. *Nat. Commun.* **4,** 2808 (2013).
7. Zheng, G. *et al.* Metasurface holograms reaching 80% efficiency. *Nature Nanotech.* **10,** 308–312 (2015).

8. Mohammadi, N. & Alu, A. Ultra-thin unidirectional carpet cloak and wavefront reconstruction with graded metasurfaces. *IEEE Antennas Wireless Propag. Lett.* **13,** 1775–1778 (2015).
9. Ni, X. *et al.* An ultrathin invisibility skin cloak for visible light. *Science* **349,** 6254 (2015).
10. Shitrit, N. *et al.* Optical spin Hall effects in plasmonic chains. *Nano Lett.* **11,** 2038–2042 (2011).
11. Yin, X. *et al.* Photonic spin Hall effect at metasurfaces. *Science*, **339,** 6126 (2013).
12. Yu, N. *et al.* Flat optics: Controlling wavefronts with optical antenna metasurfaces. *IEEE J. Sel. Top. Quant. Electron.* **19,** 4700423 (2013).
13. Aieta, F. *et al.* Out-of-plane reflection and refraction of light by anisotropic optical antenna metasurfaces with phase discontinuities. *Nano Lett.* **12,** 1702–1706 (2012).
14. Xie, Y., Konneker, A., Popa, B.-I. & Cummer, S. A. Tapered labyrinthine acoustic metamaterials for broadband impedance matching. *Appl. Phys. Lett.* **103,** 201906 (2013).
15. Li, Y. *et al.* Reflected wavefront manipulation based on ultrathin planar acoustic metasurfaces. *Sci. Rep.* **3,** 2546 (2013).
16. Tang, K. *et al.* Anomalous refraction of airborne sound through ultrathin metasurfaces. *Sci. Rep.* **4,** 6517 (2014).
17. Tang, K. *et al.* Focusing and directional beaming effects of airborne sound through a planar lens with zigzag slits. *J. Appl. Phys.* **117,** 024503 (2015).
18. Li, Y., Qi, S. & Assouar, M. B. Theory of metascreen-based acoustic passive phased array. *New J. Phys.* **18,** 043024 (2016).
19. Ding, C. *et al.* Reflected wavefronts modulation with acoustic metasurface based on double-split hollow sphere. *Appl. Phys. A* **120,** 487–493 (2015).
20. Zhai, S. *et al.* Manipulation of transmitted wave front using ultrathin planar acoustic metasurfaces. *Appl. Phys. A* **120,** 1283–1289 (2015).
21. Wang, W. *et al.* S. A. Design and demonstration of broadband thin planar diffractive acoustic lenses. *Appl. Phys. Lett.* **105,** 101904 (2014).
22. Yuan, B., Cheng, Y. & Liu, X. Conversion of sound radiation pattern via gradient acoustic metasurface with space-coiling structure. *Appl. Phys. Express* **8,** 027301 (2015).
23. Jiang, X. *et al.* Convert acoustic resonances to orbital angular momentum. *Phys. Rev. Lett.* **117,** 034301 (2016).
24. Li, Y. *et al.* Experimental realization of full control of reflected waves with subwavelength acoustic metasurfaces. *Phys. Rev. Appl.* **2,** 064002 (2014).
25. Li, Y., Jiang, X., Liang, B., Cheng, J. & Zhang, L. Metascreen-based acoustic passive phased array. *Phys. Rev. Appl.* **4,** 024003 (2015).
26. Faure, C., Richoux, O., Felix, S. & Pagneux, V. Experiments on metasurface carpet cloaking for audible acoustics. *Appl. Phys. Lett.* **108,** 064103 (2016).
27. Esfahlani, H., Karkar, S. & Lissek, H. Acoustic carpet cloak based on an ultrathin metasurface. *Phys. Rev. B* **94,** 014302 (2016).
28. Sun, S. *et al.* Gradient-index meta-surfaces as a bridge linking propagation waves and surface waves. *Nature Mater.* **11,** 426–431 (2012).
29. Sun, S. *et al.* High-efficiency broadband anomalous reflection by gradient meta-surfaces. *Nano Lett.* **12,** 6223–6229 (2012).
30. Xie, Y. *et al.* Wavefront modulation and subwavelength diffractive acoustics with an acoustic metasurface. *Nat. Commun.* **5,** 5553 (2014).
31. Ma, G. & Sheng, P. Acoustic metamaterials: from local resonances to broad horizons. *Sci. Adv.* **2,** e1501595 (2016).
32. Xu, Y., Fu, Y. & Chen, H. Steering light by a subwavelength metallic grating from transformation optics. *Sci. Rep.* **5,** 12219 (2015).
33. Larouche, S. & Smith, D. R. Reconciliation of generalized refraction with diffraction theory. *Opt. Lett.* **37,** 2391–2393 (2012).
34. Morse, P. M. & Ingard, K. U. *Theoretical Acoustics* (Princeton university press, 1968).
35. Zhao, D. *et al.* Broadband and wide-angle negative reflection at a phononic crystal boundary. *Appl. Phys. Lett.* **104,** 043503 (2014).

Acknowledgements

This work was supported by National Natural Science Foundation of China under Grant Nos 50836002 and 51176041.

Author Contributions

Bingyi Liu conceived the original idea and wrote the manuscript; Bingyi Liu and Wenyu Zhao performed the simulations and theoretical analysis. Yongyuan Jiang supervised the project.

Additional Information

Competing financial interests: The authors declare no competing financial interests.

How to cite this article: Liu, B. *et al.* Apparent Negative Reflection with the Gradient Acoustic Metasurface by Integrating Supercell Periodicity into the Generalized Law of Reflection. *Sci. Rep.* **6**, 38314; doi: 10.1038/srep38314 (2016).

Publisher's note: Springer Nature remains neutral with regard to jurisdictional claims in published maps and institutional affiliations.